



This is the accepted manuscript made available via CHORUS, the article has been published as:

## Wave propagation in square granular crystals with spherical interstitial intruders

I. Szelengowicz, P. G. Kevrekidis, and C. Daraio

Phys. Rev. E **86**, 061306 — Published 12 December 2012

DOI: [10.1103/PhysRevE.86.061306](https://doi.org/10.1103/PhysRevE.86.061306)

# Wave propagation in square granular crystals with spherical interstitial intruders

I. Szelengowicz<sup>1</sup>, P.G. Kevrekidis<sup>2</sup>, C. Daraio<sup>1</sup>

<sup>1</sup> *Graduate Aerospace Laboratories (GALCIT),*

*California Institute of Technology, Pasadena, CA 91125, USA*

<sup>2</sup> *Department of Mathematics and Statistics, Lederle Graduate Research Tower,*

*University of Massachusetts, Amherst, MA 01003-9305*

## Abstract

We investigate the propagation and scattering of highly nonlinear waves in granular systems composed of spheres in contact arranged in a square packing, and study how the presence of small and light spherical interstitial defects, also referred to as intruders, affects the wave propagation. The effects of a single defect are investigated experimentally and compared to numerical simulations, showing very good quantitative agreement. Transmitted and scattered waves are formed, whose characteristics depend on the material properties of the defect in relation to the properties of the particles in the lattice. Experiments and numerical simulations reveal that stiffer defects are more efficient at redistributing energy outside the impacted chain and soft defects induce a localization of the energy at the defect. Finally, the effects of the presence of two defects, placed diagonally or aligned in the square packing are also investigated, as well as how their interaction depends on their relative positions.

PACS numbers: 05.45.-a, 45.70.-n, 46.40.Cd

## INTRODUCTION

The propagation of nonlinear elastic waves in granular crystals, defined as elastic particles in Hertzian contact arranged in controlled geometrical packings, has received considerable attention in recent years. Granular crystals exhibit interesting dynamical properties: for example, one-dimensional (1-D) chains of spherical particles support the formation and propagation of solitary waves, [1–18], and their dynamic response can be tuned based on the amount of static precompression applied to the system [7, 14, 19–23]. There are several studies that analyze the interaction of a solitary wave with defects in a one-dimensional system [24–26], as well as the interaction of a solitary wave with different interfaces [27–34]. Interesting phenomena have been shown to occur when impurities are present in an otherwise homogeneous highly nonlinear chain of spheres, and mass defects in particular have drawn significant attention [24–26]. M. Manciu [26] studied the backscattering of a soliton-like wave as it encounters a lighter or heavier defect and suggested that the propagation of acoustic pulses could be used to detect impurities buried in granular media. The elementary interaction of light or heavy intruders with shock waves has been investigated numerically [24]. Hascoët et al. showed that a light defect acts as a secondary source of solitary waves, whereas a heavier defect is simply translated, creating a train of solitary waves forward and a stable reflected wave. When reached by a shock wave, a light defect will start oscillating between its two neighbors. Those oscillations are damped as the defect becomes a secondary source of solitary waves, and one can observe trains of solitary waves of decreasing amplitudes in both directions as the defect collides with its nearest neighbors. A heavy impurity will behave very differently: instead of exciting the defect, the shock will simply shift it in its moving direction and the chain will be halved in two parts. A stable reflected wave will propagate to the left of the defect, while the forward propagating solitary wave will be decomposed in a train of pulses. Recently, it was experimentally shown that the presence of a lighter mass defect can induce mechanical energy localization [25] as it interacts with a solitary wave. When interacting with the solitary wave, the impurity starts oscillating with a frequency which increases nonlinearly with the amplitude of the propagating pulse and decreases with the size of the impurity. The inclusion of multiple defects has also shown interesting dynamic effects [21, 28, 29, 31] and symmetry breaking phenomena [35]. One-dimensional “tapered” chains have been studied in detail and have been proposed for

the design of granular protecting devices based on the redistribution of the initial energy input [36–41].

Nesterenko numerically studied the effects of disorder in 1-D systems consisting of spheres of same material but which diameter was randomly assigned, and showed how disorder is responsible for the attenuation and decomposition of shock waves and solitary waves [1, 14]. In a more recent study, the propagation and scattering of highly nonlinear waves in disordered 1-D composite granular media was investigated [42]. It was shown that two regimes exist depending on the level of disorder. In low-disordered chains, Ponson et al. observed numerically and experimentally the propagation of a solitary pulse with exponentially decaying amplitude. As the disorder increases, the dispersion capacity of the system saturates and the wave becomes fully delocalized. Genetic algorithm methods were used to optimize the distribution of defects in a 1-D granular chain of particles in order to reduce the maximum amplitude of the transmitted signal [43].

On the other hand, the study of the dynamic behavior of ordered two-dimensional (2-D) granular crystals is relatively unexplored. There is no theoretical framework that describes the highly nonlinear wave propagation in fully 2-D systems and prior analysis of these systems consisted mostly of numerical simulations with some experiments visualizing dynamic stress in photo-elastic disks [45–47]. Velicky and Caroli studied the dependance on the external pressure of the velocities in a 2-D hexagonal packing of frictional balls, building an effective medium description taking into account local deformations due to the disorder in the ball radii [48]. The experimental testing of 2-D and 3-D systems is challenging because of the difficulty in assembling “perfect” crystals. Several studies have focused on the imperfections of granular crystals as the cause of observed deviations from the Hertzian behavior, for example [49–52]. The natural extension to the study of 1-D crystals is to explore the dynamic response of simple 2-D square packings (pseudo 1-D systems) [53]. Leonard and Daraio showed that, depending on the type of excitation imparted on the system (location, number of particles impacted, temporal duration of the impact), solitary waves can form in one or several different chains within the square array. The presence of interstitial particles uniformly distributed in the packing (i.e., effectively forming a centered squared granular lattice) has been shown to force the system to distribute stress in 2-D fronts, whose properties can be tailored by the selection of the particles material properties [54, 55].

It is important to note that the presence of defects in 1-D chains is limited to the pres-

ence of particles of different sizes, materials, or shapes placed in the chain in contact with neighboring particles [24–26]. In 2-D, this definition needs to be extended as it is also possible to add particles on off-grid positions. In addition, 2-D systems allow for the presence of vacancies (i.e., lattice points with no particles) without completely disrupting the wave propagation. In this paper, we describe the interaction of highly nonlinear solitary waves with a single interstitial defect particle, using experiments and numerical simulations to study the effects of force and energy redirection, reflection and trapping, as a function of the defect’s materials properties. We also describe the interaction between two defects, as a function of their relative position in the lattice.

Our presentation is structured as follows. In section II, we present the experimental and numerical setup at hand. In section III, we examine the case of a single defect (also of different stiffness and density characteristics). It is seen that the stiffer the defect, the more it favors the redistribution of the energy in the system. A rigid body collision model is also used based on the energy and momentum conservation to establish a reasonable approximate estimate of the resulting distribution of the relevant energy fractions. Finally, the case of two interstitial defects is considered in section IV, both in the special setting where they are in contact with the same particle, enhancing the number of directions that receive an observable fraction of the pre-collision energy, and in that where they are more separated. In the latter case, the intruders can be thought of as acting independently. Finally, in section V, we present some conclusions and possibilities for further study.

## EXPERIMENTAL AND NUMERICAL SETUPS

Our 2-D experimental setup is composed of a flat polycarbonate base and four movable delrin walls to support the particles. We assemble a 20 by 20 square packing using  $2R = 19.05$  mm diameter stainless steel spheres (nonmagnetic, 316 type). The defect particles consist of custom made spheres that fit exactly in the interstitial sites. We studied the effects of several different materials for the defect particles: tungsten carbide (TC), 316 stainless steel, brass alloy 260 and polytetrafluoroethylene (PTFE). The material properties of the defect particles studied are summarized in Table I. Due to the size of the interstices, the intruder particles are smaller than the beads of the square packing:  $R_{defect} = (\sqrt{2} - 1)R$ . In order to have all the centers of mass of the particles in one horizontal plane, the defects are

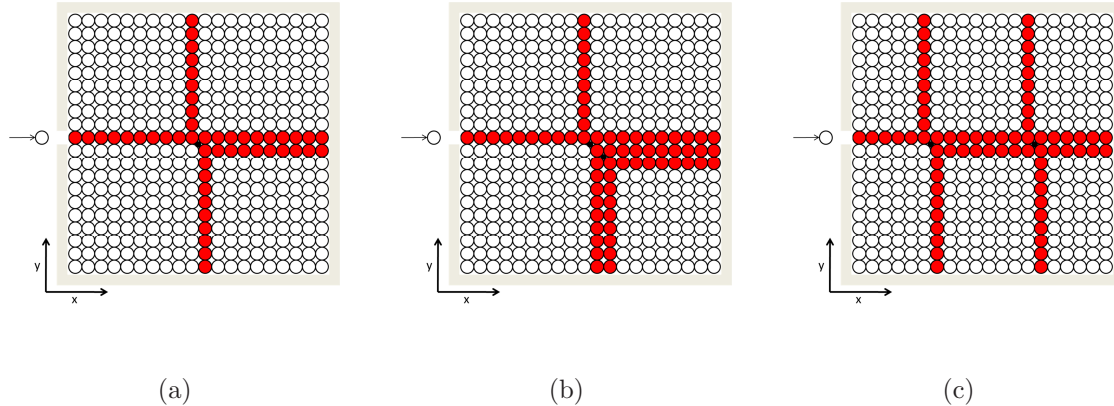


FIG. 1: (Color online) Schematic diagrams of the different system configurations studied. (a) Single defect case: a spherical intruder (black particle) is included in the center of a 20 by 20 square packing composed of stainless steel spheres confined by four delrin walls. The system is impacted by a steel particle identical to the other particles in the lattice, exciting a single row of spheres from the left side. (b) Configuration including two defects placed diagonally, adjacent to the same particle. (c) Configuration including two defects placed along the same row of particles. In all panels, the red (grey) color identifies the particles involved in the wave propagation (reflections not taken into account).

	TC	Stainless steel	Brass	PTFE
(kg/m <sup>3</sup> ) $\rho$	15800	8000	8500	2200
(GPa) E	400	193	103	1.26

TABLE I: Densities and Young's moduli of the different materials used in our experiments and numerical simulations.

placed on cylindrical PTFE stands. The system is impacted on one side by a single striker particle identical to the particles forming the square packing and its velocity is measured with the use of an optical velocimeter. The different particle arrangements considered in this study are reported in Fig. 1.

Custom sensor particles were built using mini tri-axial accelerometers (PCB 356A01 sensitivity  $0.51mV/(m/s^2)$ ) embedded within spherical particles placed in positions of interest in the setup (see [53] for a more complete description). The accelerometers are connected to a signal conditioner (PCB 481A02) and a data acquisition board (NI BNC-2110 and NI PCI-6123) with a 500 kS/s simultaneous sampling rate.

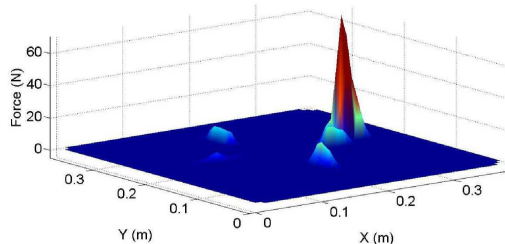


FIG. 2: (Color online) Force versus position map obtained from the simulation of the dynamics of a system composed by a steel intruder in a steel square packing at  $t=0.6\text{ms}$ . The origin of time is the impact of the system at coordinates  $(X=0.0, Y=0.2)$  by a steel striker particle with initial velocity  $0.2\text{m/s}$ . After interaction of the incoming solitary wave with the defect, the transmitted, reflected and scattered solitary waves are evident.

We numerically model the square packing of 400 spherical beads plus one or two interstitial spherical defects and a striker bead with (conservative) Hertzian interactions between particles:

$$\ddot{u}_i = - \sum_{\langle j \rangle} A_{i,j} [(u_i - u_j) \cdot \vec{e}_{ij}]_+^{\frac{3}{2}} \vec{e}_{ij}, \quad (1)$$

where  $u_i$  is the vectorial displacement of the  $i^{\text{th}}$  particle from its equilibrium uncompressed position,  $A_{i,j} = \frac{2}{3} \sqrt{\frac{R_i R_j}{R_i + R_j}} \left( \frac{1 - \nu_i^2}{E_i} + \frac{1 - \nu_j^2}{E_j} \right)^{-1}$  and  $\vec{e}_{ij}$  is the unit vector connecting the centers of beads  $i$  and  $j$ , oriented from  $i$  to  $j$ ; the symbols  $\langle j \rangle$  denote that  $j$  needs to be a nearest neighbor to  $i$ .  $[X]_+$  denotes the positive part of  $X$  as no interaction exists between particles when they lose contact. Numerical simulations are run using a fourth order Runge-Kutta integration scheme to solve the equations of motion of all the particles. The striker particle impacts one side of the square array and its velocity is determined from experiments. All other particles start at rest in their equilibrium positions.

The acceleration values measured experimentally are compared to the values obtained from numerical simulations. However, when comparing numerical results with experiments, several factors can account for discrepancies. The most important one is the presence of dissipation in the real system, which is responsible for a decrease in amplitude, and hence velocity, of the traveling waves. Dissipative losses are not taken into account in our numerical

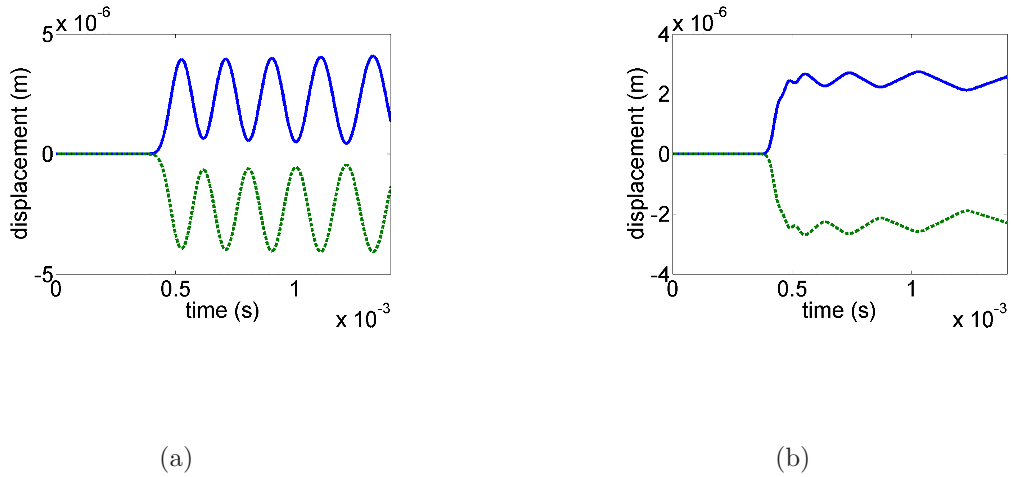


FIG. 3: (Color online) Numerical results showing the displacement of the defect particle as a function of time when it is made of (a) PTFE and (b) stainless steel. In both cases, the solid blue curve represents the displacement of the defect particle in the x-direction and the dashed green curve represents the the displacement of the same particle in the y-direction.

computations. Another one is the variability intrinsic to real systems: the particles used in experiments are not perfect, and a slight tolerance variation on their diameters can cause irregularities in the contact network, such as local losses of contact or precompressions.

## SINGLE DEFECT

The first system studied is presented in Fig. 1(a). A spherical defect is placed in the center of a uniform steel square packing, and a horizontal chain in contact with the defect is impacted by a steel sphere. Without the presence of the intruder, the system would behave as an effectively 1-D system, i.e., one in which the excitation only propagates along its initial direction. However, the presence of the defect adjacent to the impacted chains modifies the dynamic response of the system: after the incoming solitary wave interacts with the defect, we observe one reflected, one transmitted and three scattered waves (see Fig. 2), whose properties depend on the material properties of the defect. A single solitary wave is always transmitted down the impacted chain after the defect. This is due to the fact that the first bead after the intruder in the impacted chain loses contact with both its left neighbor and the intruder. We numerically evaluate the scattered energy by calculating

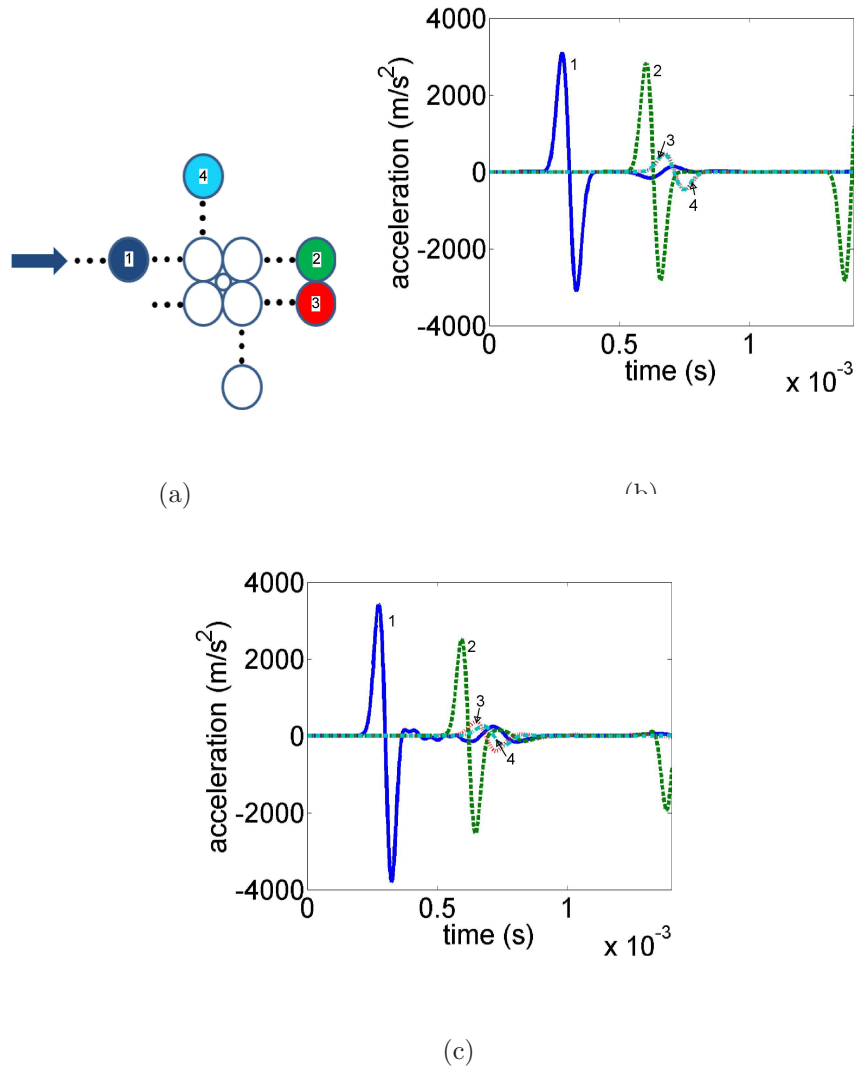


FIG. 4: (Color online) Single stainless steel defect configuration, impacted by a stainless steel sphere of diameter 19.05 mm, with initial velocity 0.19 m/s. (a) Simplified schematic diagram representing the particles located around a single spherical intruder. The colors and labels of the particles correspond to the colors and labels of the acceleration curves in panels (b) and (c). The arrow on the left represents the impact direction. (b) Numerical results showing the particles’ acceleration as a function of time for the incoming and reflected wave (solid dark blue curve labeled “1”, 4 particles away from the defect), the transmitted wave (dashed green curve labeled “2”, 5 particles away from the defect) and the scattered waves (dotted red and turquoise labeled “3” and “4”, 5 particles away from the defect). (c) Experimental results corresponding to (b).

the difference between the input energy and the energy carried by the transmitted solitary

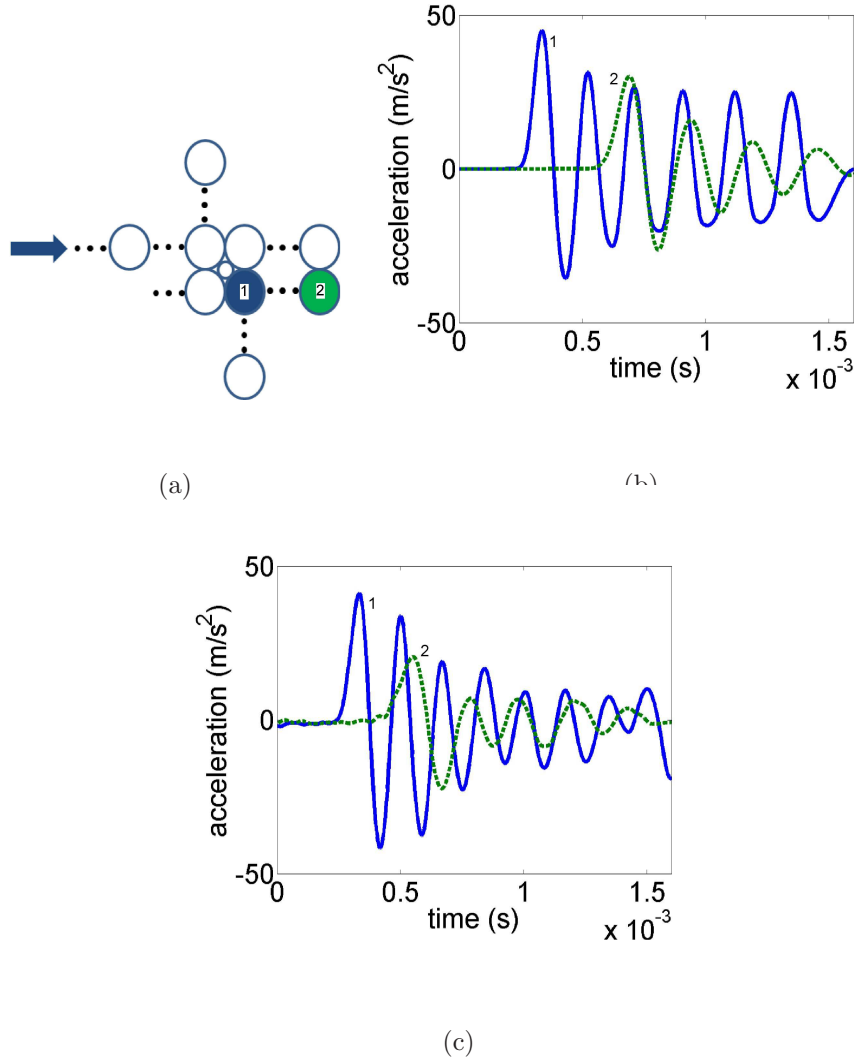


FIG. 5: (Color online) Single PTFE defect configuration, impacted by a stainless steel sphere of diameter 19.05 mm, with initial velocity 0.23 m/s. (a) Simplified schematic diagram representing the particles located around a single spherical intruder. The colors and labels of the particles correspond to the colors and labels of the acceleration curves in panels (b) and (c). The arrow on the left represents the impact direction. (b) Numerical results showing the particles’ acceleration as a function of time for a particle immediately adjacent to the defect (solid blue curve labeled “1”) and 5 particles away (dashed green curve labeled “2”). (c) Experimental results corresponding to (b).

wave. We refer to the chains in which waves are propagating as “impacted”, “adjacent”, “top” and “bottom” chains, colored in red on Fig. 1(a). After the incoming wave reaches

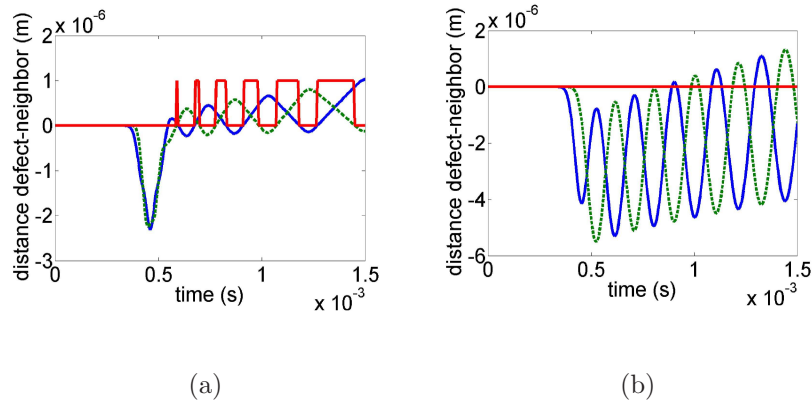


FIG. 6: (Color online) Numerical results showing the horizontal displacement of the defect particle for the (a) stiff (steel) and (b) soft (PTFE) defect configurations, relative to its two active neighbors (top left and bottom right particles adjacent to the defect particles). The solid blue curve represents the relative displacement in the x-direction of the defect particle with respect to its top-left neighbor and the dashed green line with respect to its bottom-right neighbor. Note that we do not show the relative displacement in the y-direction since it is equal to the relative displacement in the x-direction. The two particles are compressed against each other when the curves are negative and they are not in contact when positive. The red step-curve is non zero when a complete loss of contact occurs between the defect and its two active neighbors.

the defect particle, the defect’s motion is observed to be identical in the x and y directions. This is shown in Fig. 3 where one can see that the two components of the displacements of the defect particle are equal and opposite. This is due to the fact that the center of mass of the intruder is placed along the line connecting the centers of mass of its top-left and bottom-right neighbors (at a  $45^\circ$  angle with the x-axis). We consequently observe, both experimentally and numerically, identical signals propagating down the “adjacent” and “bottom” chains. When the transmitted waves are reflected back from the boundaries they excite the intruder again, and cause its motion to become disordered. In this study, we limit our analysis to the interaction of the defect with the incoming wave, neglecting the effects of reflections.

First, we numerically investigated the effect of variations of the defect’s mass and stiffness on the energy redirection through the crystal, for different impact velocities. We showed that the defect’s mass has very little effect on the maximum amplitude of the signal transmitted beyond the defect particle in the direction of impact, relative to the input energy. However,

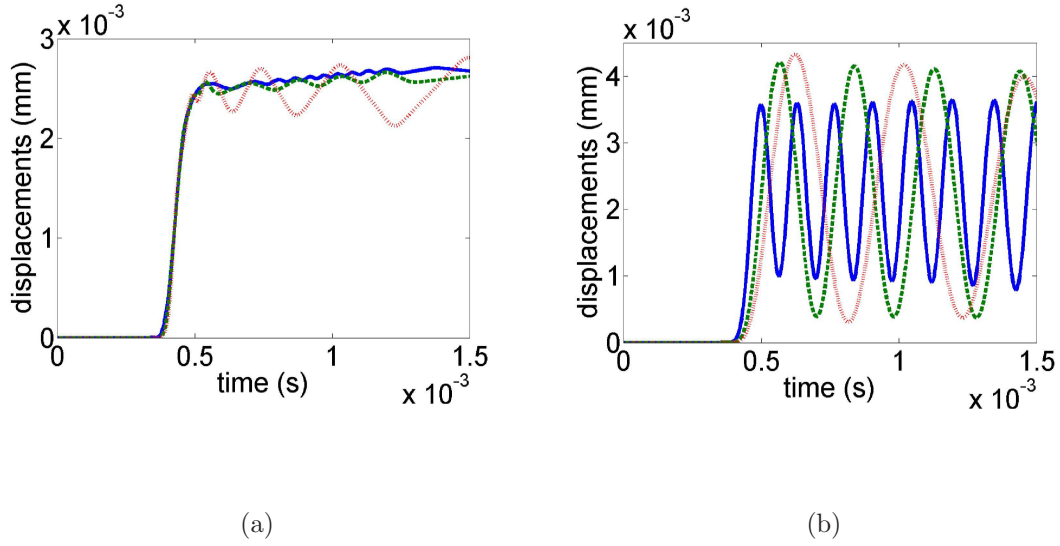


FIG. 7: (Color online) Numerical results showing the effect of density variation on the defect particle's displacement in the horizontal direction (along the striker direction). Note that we do not show the displacement in the y-direction since it is equal to the displacement in the x-direction. The numerical results are obtained from idealized particles in which the elastic modulus ( $E$ ) is kept constant, and the density is varied arbitrarily. (a) stiff ( $E = 193 \text{ GPa}$ ) and (b) soft ( $E = 1.26 \text{ GPa}$ ) case. The density values considered in both panels are:  $d = 1000 \text{ Kg/m}^3$  (solid blue),  $d = 4000 \text{ Kg/m}^3$  (dashed green) and  $d = 8000 \text{ Kg/m}^3$  (dotted red) curves.

the defect's stiffness can play a nontrivial role in the interactions: the stiffer the defect, the more energy is redirected from the impacted chain to other parts of the system.

### Single steel defect

The results obtained for a lattice composed of stainless steel particles and a single stainless steel defect are shown in Fig. 4. It is evident that the system supports the formation and propagation of a single solitary wave, and that the solitary wave's interaction with the defect results in a small amount of energy redirected from the impacted chain to two solitary waves propagating sideways and, partially, to a single solitary wave reflected backward. We find excellent agreement between numerical and experimental results (compare Fig. 4(b) with Fig. 4(c)). However, the presence of dissipative losses in experiments is evident from the decreasing wave amplitude of the traveling waves. For this configuration, numerical

calculations show that 14.32% of the input energy is transmitted to other parts of the system and does not travel along the impacted chain after the intruder (4.15% is deflected up, 4.30% down, 4.30% in the adjacent chain and 1.57% reflected).

### **Single PTFE defect**

The results obtained for the lattice composed of stainless steel particles and a single PTFE defect are shown in Fig. 5. In this case, the interaction of the incoming solitary wave traveling in the impacted chain with the soft intruder leads to the formation of trains of solitary waves of decreasing amplitudes in the “top”, “bottom” and “adjacent” chains, and we also observe a train of solitary waves of small amplitude reflected backward. When reached by the incoming solitary wave, the PTFE intruder is strongly compressed between its top-left and bottom-right neighbors, and starts oscillating between them. As it oscillates, the PTFE intruder slowly pushes its neighboring particles away from it, bouncing back and forth. The energy of the intruder progressively decreases as multiple solitary waves are formed in all four directions, resulting in the trains of waves observed numerically and experimentally. For this configuration, numerical calculations show that only 1.23% of the input energy is transmitted to other parts of the system and does not travel along the impacted chain after the intruder. For comparison, a stiffer tungsten carbide intruder deflects 17.7% of the total input energy, while a softer brass intruder deflects 11.33% of the input energy.

### **Relative displacements**

The relative displacements of the defect particle with its neighbors are shown in detail in Fig. 6 for the particle configurations analyzed in Fig. 4 and Fig. 5. For the packing including a single steel defect (Fig. 6(a)), it is evident that the top-left neighbor compresses the defect particle, which in turn compresses its bottom-right neighbor, and all three particles are translated (at time = 0.4-0.6 ms). After this translation the intruder loses contact, first with its first neighbor, and quickly thereafter also with its second, and then bounces back and forth between the two. The two neighbors slowly become more and more distant from each other and the defect also carries less velocity having imparted progressively more of it through subsequent collisions. This leads eventually to “individual” interactions of the

defect with each one neighbor at a time, mediated by longer travel times during which the defect is in contact with neither of its neighbors. The relative displacement between the defect and its neighboring particles is always small (0.2 microns) and these interactions give rise to small secondary waves propagating laterally and in the row of particles adjacent to the impacted one. This picture (of a sequence of collisions with top left and bottom right neighbors) will also form the basis for our rigid body collision model theoretical analysis of the relevant phenomenology presented below. For a soft PTFE intruder (Fig. 6(b)), we observe that the first interaction with the first neighbor causes the intruder to be strongly compressed between the two bigger and stiffer steel spheres. The intruder oscillates between the two particles with a frequency of oscillation being a nonlinearly increasing function of the amplitude of the incoming wave. The two stiff neighbors are slowly pushed away by the intruder, and a train of solitary waves is transmitted after the defect in the row of particles adjacent to the impacted one.

### **Effect of density**

Numerical simulations were run to investigate the role of density independently of the role of stiffness of the defect particles. We created idealized particles, in which we varied the particle density while maintaining a constant stiffness value. For these cases, we plot the displacement of the intruder particle to show the variations in the dynamics of the systems. Because of the symmetry of the system, the x- and y-displacements of the intruder have equal norms. In Fig. 7 we present the x-displacement (i.e., horizontal displacement) of the defect particle for both a stiff ( $E = 193GPa$ , Fig. 7(a)) and a soft ( $E = 1.26GPa$ , Fig. 7(b)) material, varying the density in each case. We note that as the incoming solitary wave reaches a stiff defect from its top left neighbor, the defect is forced to translate laterally. This translation is followed by small oscillations of the defect between its top left and bottom right neighbors, during which the defect alternately loses contact between them. In this scenario, the incoming solitary wave is decomposed into transmitted, reflected and scattered solitary waves, and the secondary oscillations result in small amplitude trailing waves. When the incoming solitary wave reaches the softer defect, we observe a transition to a different dynamic regime in which the defect particle starts oscillating immediately, without a lateral translation (see Fig. 7(b)). In this case, the defect is compressed between

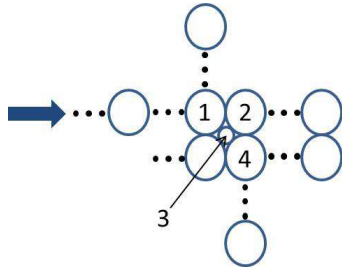


FIG. 8: (Color online) Numbering of the particles involved in the calculation of the rigid particle model.

its two active neighbors (top left and bottom right) and the large amplitude of oscillations is due to the larger deformations of the soft intruder between the steel particles. Energy is localized similarly to what was observed in one-dimensional systems [25], and the defect particle excites secondary solitary waves. The formation of transmitted trains of solitary waves, observed both numerically and experimentally, are shown in Fig. 5.

### Rigid body collision model

For the case of stiff defects where we observe transmitted, scattered and reflected solitary waves (as opposed to trains of solitary waves for soft defects), a natural model has been developed to estimate the percentages of the input energy traveling in the top, bottom, impacted and adjacent chains after interaction of the intruder with the incoming solitary wave. We assume the spherical particles (see numbering in Fig. 8) to be rigid bodies undergoing elastic collisions. This approach is a simplification for the interaction of a multi-particle wave with the interstitial defect. A similar approach was taken in the independent collision model of [36]. This approach is exact for perfectly rigid spheres and a good approximation when the collision durations are short in comparison to the time between two collisions, and was later used in [37, 39] for the description of tapered chains. The analytical results obtained with this approximation were found to be in very good agreement with the full field numerical model (which considered energy and momentum exchanged between all the particles in the system).

We first consider the interactions between particles 1, 2 and 3, and denote by  $m$  and  $m_d$

the masses of the particles in the packing and the defect respectively. The superscripts  $i$ ,  $t$ ,  $r$  and  $u$  represent the incoming, transmitted, reflected and scattered in the up direction velocities respectively. Using the conservation of momentum and kinetic energy, we obtain the following system of equations:

$$\begin{aligned}
mv^{(1i)} &= -mv^{(1r)} + mv^{(2t)} + \frac{\sqrt{2}}{2}m_d v^{(3t)} \\
mv^{(1u)} &= \frac{\sqrt{2}}{2}m_d v^{(3t)} \\
\frac{1}{2}mv^{(1i)^2} &= \frac{1}{2}mv^{(1r)^2} + \frac{1}{2}mv^{(1u)^2} + \frac{1}{2}mv^{(2t)^2} + \frac{1}{2}m_d v^{(3t)^2}
\end{aligned} \tag{2}$$

We numerically observe that the amplitude of the reflected wave is small with respect to the other scattered and transmitted waves (see Fig. 4). This is due to the fact that  $m_d$  is small with respect to  $m$  and we consequently neglect  $v^{(1r)}$  in our analysis. Eq. 2 then yields:

$$\begin{aligned}
v^{(1u)} &= \frac{m_d}{m + m_d}v^{(1i)} \\
v^{(2t)} &= \frac{m}{m + m_d}v^{(1i)} \\
v^{(3t)} &= \sqrt{2}\frac{m}{m_d + m}v^{(1i)}
\end{aligned} \tag{3}$$

Assuming that all the energy of  $v^{(2t)}$  forms the transmitted part in the direction of the initial excitation, we obtain the transmitted energy fraction for the homogeneous case as:

$$\frac{E_t}{E_i} = \frac{\frac{1}{2}mv^{(2t)^2}}{\frac{1}{2}mv^{(1i)^2}} = \left( \frac{1}{1 + (\sqrt{2} - 1)^3} \right)^2 = 87.17\% \tag{4}$$

This is in good agreement with the numerical results for the same case (85.68%). The contribution to the energy deflected up is  $\frac{\frac{1}{2}mv^{(1u)^2}}{\frac{1}{2}mv^{(1i)^2}} = \left( \frac{(\sqrt{2}-1)^3}{1+(\sqrt{2}-1)^3} \right)^2 = 0.44\%$ .

We consider thereafter the interactions of the defect (which has velocity  $v^{(3t)}$ ) with particles 1 and 4. We remind the reader that the motion of the intruder being along the diagonal, it is unnecessary to consider the interactions with particle 2 and also with the intruder's bottom-left neighbor. We model the transmission of the energy from the intruder to its two active neighbors by an infinite series of instantaneous elastic collisions. Denoting by  $v^{(3tr)}$  and  $v^{(4t)}$  the velocity of the intruder and the velocity transmitted to particle 4 after their

	up	refl	adj	bottom	trans
Rigid particle model	3.10	2.66	3.54	3.54	87.17
Numerical	4.15	1.57	4.30	4.30	85.68

TABLE II: Comparison of the percentages of the input energy redirected in the system in the rows and columns of spheres adjacent to the defects for the rigid particle model and numerical calculations. We define energy “up” as the energy redirected upward in the column of particles above the first defect, “reflected” as the energy reflected back in the impacted chain, “adjacent” as the energy redirected in the right direction in the row adjacent to the impacted chain, “bottom” as the energy redirected downward in the column of particles below the first defect and “transmitted” as the energy transferred in the impacted chain after the defect.

first collision, conservation of momentum and kinetic energy yields:

$$\begin{aligned}
 v^{(4t)} &= \frac{2m_d}{m_d + m} v^{(3t)} \\
 v^{(3tr)} &= \frac{m_d - m}{m_d + m} v^{(3t)}
 \end{aligned}
 \tag{5}$$

After this first interaction of the intruder with particle 4, another collision happens between the intruder and particle 1, and so on. Notice that this is exactly in line with the observations of Fig. 6(a). Summing the contributions of all the collisions, one can calculate the energy fractions transmitted to particle 1 and 4:

$$\begin{aligned}
 \frac{E_4}{E_i} &= \frac{8(mm_d)^2}{(m_d + m)^4} \sum_{k=0}^{\infty} \left( \frac{m_d - m}{m_d + m} \right)^{4k} \\
 \frac{E_1}{E_i} &= \frac{8(mm_d)^2}{(m_d + m)^4} \sum_{k=0}^{\infty} \left( \frac{m_d - m}{m_d + m} \right)^{4k+2}
 \end{aligned}
 \tag{6}$$

We finally assume that the energy transmitted to particle 4 will be split equally between the adjacent and the bottom chains. Similarly, the energy transmitted to particle 1 by the intruder is assumed to be split equally between the top chain and the impacted one (before the intruder). Hence, adding the contributions of the first part of the calculation, we can find the transmitted, scattered and reflected energy fractions, in fairly good agreement with the numerical simulations. The results from this calculation as well as the numerical ones are summarized for the case of a stainless steel intruder in Table II.

Understanding how a single spherical intruder interacts with a solitary wave is the first step towards the understanding of more complex dynamics that appear when several defects

are present. In the next section, we investigate the interaction of two spherical intruders when placed in a square packing, for

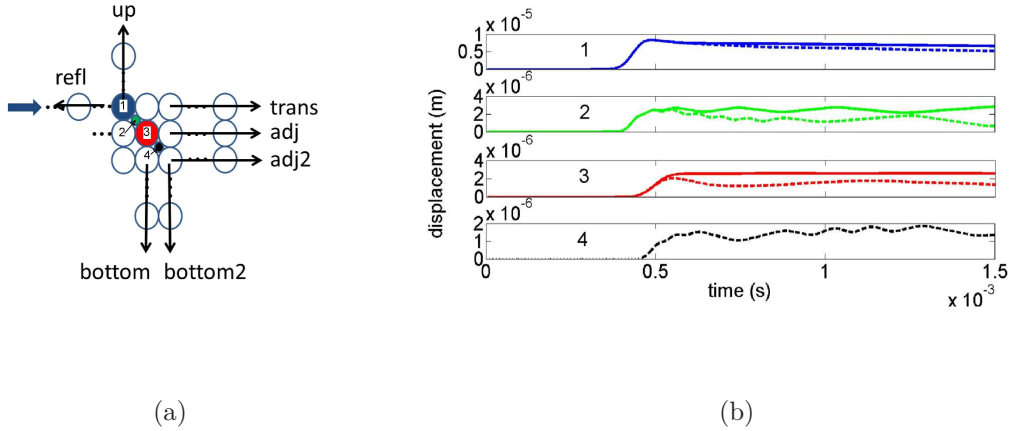


FIG. 9: (Color online) Numerical results showing the horizontal displacement of the particles involved in the impulse redirection when two stainless steel intruders are located in a square packing of stainless steel spheres impacted from the left by a steel particle. (a) Schematic diagram of the particles configuration. The arrows indicate the labeling of the different chains of interest (where a signal is propagating). (b) Displacements of the four numbered (and colored) particles in (a). On each plot, the solid line corresponds to the results obtained when only a single defect is present in the packing, and the dotted lines correspond to the results obtained when two defects are present in the packing. The colors and labels of the particles correspond to the colors and labels of the displacement curves in panel (b).

## TWO DEFECTS

We study the effects of the presence of two defects in the lattice, as a function of their relative position. As seen in the first part of this manuscript, when a single solitary wave interacts with a single defect, the energy is redistributed only along the few chains adjacent to the defect. If two defects are located sufficiently far apart from each other in the granular crystal, we expect their individual behavior to be independent of each other, and similar to that of a single defect, without any dynamic interactions between them. However, when the two defects are sufficiently close to each other, the dynamic behavior of the granular crystal

is expected to be dependent on the interaction between the two defects.

### **Two defects in contact with the same particle**

In this section, we study the effect of two defects placed diagonally to each other, but adjacent to the same particle in the crystal (Fig. 1(b)). Similarly to the case where one defect only is present, the positions of the intruders with respect to their direct neighbors will cause them to move along the diagonal connecting the centers of mass of particle 1 and 3 (see Fig. 9(a)). The x-displacement and y-displacement of the first intruder are hence equal, as are the x-displacement and y-displacement of the second intruder. It is important to remember that this symmetric behavior is preserved only before the waves reflected from the boundary of the system reach the intruders, after which their motions become disordered. Similarly to the analysis performed for the single defect case, we numerically calculate the total energy redirected from the impacted chain by subtracting the energy carried by the solitary wave in the impacted chain after the defects from the input energy. We restrict our analysis to the case of stiff intruders. We show that the dynamic behavior of the first defect is very similar to the dynamic behavior observed in a lattice with a single defect of the same material. This can be seen comparing the displacement of the first intruder in the x-direction with the displacement of a single defect occupying the same interstice (see Fig. 9). However, the presence of a second active defect provides extra stiffness in the system, resulting in a reduction of the amplitude of oscillations.

The addition of a second defect placed diagonally with respect to the first one does not have a significant effect on the energy dispersion. We calculate numerically how the input energy is redistributed in the different chains of the system. For the sake of simplicity, we consider only the cases with stiff defects - stainless steel and tungsten carbide (TC) - for which energy localization can be neglected. The two additional chains in which solitary waves are going to propagate due to the second defect are referred to as “adjacent2” and “bottom2”. Because a second defect stiffens the contact between the first defect and its bottom right neighbor, more energy is scattered upward and reflected backward. The results for the steel/steel and steel/TC are presented in Table III.

Case	up	refl	adj	adj2	bottom	bottom2	trans
Steel (num)	4.15	1.57	4.30	0.00	4.30	0.00	85.68
Steel/TC (num)	4.69	2.05	2.53	1.28	2.53	1.28	85.65
Steel/steel (num)	4.64	2.00	2.86	1.00	2.86	1.00	85.65
Steel/steel (model)	3.98	3.54	1.16	1.50	1.16	1.50	87.17

TABLE III: Percentages of the input energy redirected in the system in the rows and columns of spheres adjacent to the defects. We define energy “up” as the energy redirected upward in the column of particles above the first defect, “reflected” as the energy reflected back in the impacted chain, “adjacent” as the energy redirected in the right direction in the row adjacent to the impacted chain, “adjacent2” as the energy redirected in the right direction two rows below the impacted chain, “bottom” as the energy redirected downward in the column of particles below the first defect, “bottom2” as the energy redirected downward in the row below the second defect and “transmitted” as the energy transferred in the impacted chain after the defect. The first three rows of the table show the numerical results for three different cases: the single steel defect case, the cases where a second tungsten carbide defect is placed diagonally with respect to the first one, or the case where a steel defect is placed diagonally with respect to the first one. The last row corresponds to the semi-analytical rigid body collision model for the case of 2 steel defect particles.

### Rigid body collision model

For this entire section, we use the numbering depicted in Fig. 9(a). While this configuration appears to be only slightly more complicated than the single defect configuration, adapting the rigid body collision model presents significant challenges. This is because of the intricate effects of backscatter of beads 2 and 4 and their interplay, especially with bead 3. The beginning of the calculation is similar to what was done for the modeling of the interaction of a single defect with a solitary wave: particle 1 first interacts with its right neighbor in the impacted chain and particle 2, and we once again make the assumption to neglect any reflected energy during this first interaction. The transmitted energy is identical to the single defect case (87.17% of the input energy) as this model does not include any stiffening of the contact between the first defect particle and its bottom right neighbor. Particle 2 then interacts with 3 (and 1) which subsequently partitions its energy between 4 and the

”adjacent” and ”bottom” chains. In order to describe the following collisions, it is useful to look at the numerical results presented in Fig. 9(b). After the first interaction of particle 2 with particle 1, the former starts oscillating between particles 3 and 1 (green dashed curve labeled “2” between 0.6 and 0.8 *ms*) as particle 3 is being pushed towards the second defect. The second defect then starts to oscillate between particles 3 and 5 and particle 3 is pushed back towards the second defect (see black curve labeled “4” between 0.8 and 1.3 *ms*), and so on. We consequently consider that the two defects are interacting independently and in an alternative fashion with particle 3, for about 4 oscillations each time (inferred from Fig. 9(b)). We also assume that the energy of particle 1 is evenly distributed in the ”up” and ”reflected” chains, whereas the energy of particle 5 is split between the “adjacent2” and “bottom2” chains (see Fig. 9(a)). The results are presented in the last row of Table III along with the numerical simulation data, and are in fairly good agreement with one another. This approach clearly underestimates the input on the ”adjacent” and ”bottom chains”, as the only contribution in our model comes from the first collision of particle 3 with particle 4 and these two chains, yet is the best we can presently do without using too much feedback from the numerical simulations. We find the relevant analysis to be instructive as a lower bound of the corresponding energy partition complementing the transmitted portion of 87.17%.

### **Two defects in a line**

We study the dynamic response of the granular system, when two defects are placed along the same row of spheres, parallel to the impacted chain. The schematic diagram of this configuration is presented in Fig. 1(c). We restrict our study to the case of a steel square packing with two tungsten carbide intruders, impacted by a steel particle. We note that the response of the system is dependent on the relative distance of the defects in the packing: if the two defects are located far from each other, the behavior of the system is similar to that observed for a single defect. In this case, after an incoming solitary wave interacts with the first defect, two solitary waves propagate towards the second defect: a transmitted wave traveling in the row of particles impacted by the striker, and a redirected wave, traveling in the row of particles parallel to it (and immediately below it). According to what was shown in the single defect case, these two waves have different amplitudes, and hence different velocities. Consequently, these waves reach the second defect separately, and

the two defects act independently of each other. The energy redirection properties of the system are greatly improved as we observe a geometrical decrease of the leading traveling energy in the impacted chain: as shown in the single defect study, a TC intruder deflects 17.7% of the total input energy. This corresponds to 82.3% of the total initial energy propagating in the impacted after the first intruder. 67.7% (or 82.3% of the remaining energy) of the total initial energy will propagate in the impacted chain after the second TC intruder, and so on if more intruders are present. Hence, it is possible, for sufficiently many well separated intruders to obtain a transmitted energy fraction as small as desired according to the following prescription. To ensure that the transmitted fraction is smaller than  $\alpha$ , then the number of intruders  $N$  that must be used is  $N \geq \lceil \log(\alpha)/\log(0.823) \rceil$ , where the bracket stands for the integer part.

If the two defects are sufficiently close, the waves transmitted in the impacted chain after the first intruder and in the chain parallel to it will not reach the second intruder separately. This leads to more complex dynamics of the second intruder as it interacts with two solitary waves of different amplitudes at the same time. Moreover, the two solitary waves reach the second intruder from different sides (which is also true when the two defects are far apart), inducing a disordered motion as the defect is simultaneously pushed up and down with different forces.

Numerical calculations and experiments were run to estimate the minimum spacing  $l$  necessary for two defects to be independent. This distance is expected to depend on the velocity of impact, as well as the material of the defect particles, which both affect the velocity of the transmitted and forward scattered solitary waves. We denote by  $r_t$  the force amplitude ratio between the amplitude of the wave transmitted in the impacted chain after the intruder and the amplitude of the incoming wave (in the impacted chain before the intruder), and  $r_s$  the force amplitude ratio between the amplitude of the wave redirected in the chain parallel to the impacted chain and the amplitude of the incoming wave. Assuming that the force-velocity scaling relation  $v \propto F^{1/6}$  [14] is valid for effectively one dimensional systems [53], we obtain the following relationship relating the incoming signal velocity  $v$  to the transmitted wave velocity  $v_t$  and the redirected wave velocity  $v_s$ :

$$v_t - v_s = (r_t^{1/6} - r_s^{1/6})v. \quad (7)$$

In order to verify that the pulses detected in our system are solitary-like, we monitored the

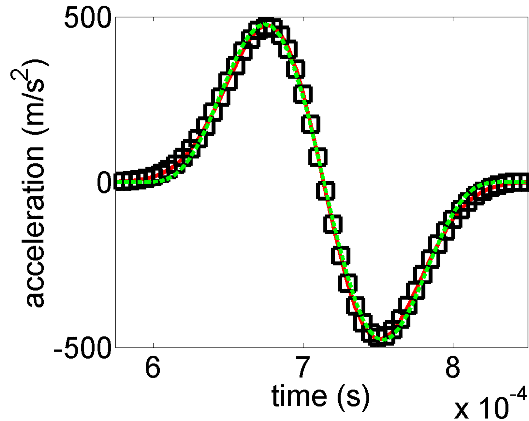


FIG. 10: (Color online) Comparison of the shape of the acceleration signals propagating in the “adjacent” chain after the defect particle with the analytical solution obtained by Nesterenko for 1-D homogeneous systems. The solid red curve (resp. black square makers) represents the signal observed 5 (resp. 9) particles after the intruder. The green dashed curve shows Nesterenko’s analytical solution.

shape of the propagating signals before and after the interaction with the defect. We noted that the pulse shape remains constant as it travels down the various chains. An example is given in Fig. 10 where we compare the shapes of the acceleration signal in the “adjacent” chain 5 particles after the intruder (solid red curve) and 9 particles after the defect (black square markers). As one can see, their shapes are identical and the two curves completely overlap. We also compared the shape of these two curves to the predicted analytical shape for a solitary wave (the Nesterenko’s solution obtained for 1-D homogeneous systems - green dashed curve in Fig. 10). We observe that the shapes of the two signals (numerical solution and analytical solution) are very close. At the intuitive level, this can be justified as follows. For each row of the two dimensional chain, the traveling wave propagates without affecting the other rows (as an effectively one-dimensional entity). Hence, both before and after the interstitial defect, we have effectively quasi-one-dimensional chains along which genuine traveling waves can propagate. The only redistribution of energy occurs at the defect, which routes that energy into transmitted (along the various directions, as explained by the particle model) and reflected. Once this routing process is completed, naturally the energy reorganizes itself into traveling waves along these effectively one-dimensional directions. It

is consequently justified to use the scaling relation previously mentioned.

Since the velocity of the incoming wave depends weakly on the force amplitude, and hence on the velocity of impact, we expect to see a small effect of the impact velocity on  $l$ . The two ratios  $r_t$  and  $r_s$  depend on the Young's modulus of the intruder  $E_{defect}$ ,  $r_t$  being a decreasing function and  $r_s$  an increasing function of  $E_{defect}$ , so that  $l$  increases with  $E_{defect}$ . For the range of impact velocities experimentally investigated (0.05 to 0.2 m/s),  $l$  was found to be around 9-10 particle diameters. Numerical and experimental results are shown in Fig. 11 and Fig. 12, for the two cases where the defects are eight and ten interstices apart. As one can see, when located eight interstices away from each other, one cannot distinguish between the end of the first wave and the beginning of the second one (red curve). This becomes possible, however, when the spacing is set to ten interstices. When placed closer to each other, the two defects start to interact, and the behavior of the second defect becomes more complicated, as its interaction with the (fast) transmitted wave and the (slow) scattered wave in the adjacent chain overlap. Preliminary numerical and experimental results showed that in the extreme case where spherical defects are located in all interstitial spaces in a line, one can achieve coupling of the impacted and adjacent chain and equipartition of the input energy in those two chains.

## CONCLUSION

In this paper, the interaction of a solitary wave with spherical interstitial defects placed in an uncompressed, 2-D square packing of stainless steel spheres is studied, investigating in a first time the effect of a single defect in the packing. The numerical calculations and experimental results show that spherical defects redirect part of the impact energy, in four directions along the rows and columns of particles in contact with the defect. The defect particle's stiffness plays an important role in the impact energy redirection in the system, and the mass of the defect and the velocity of impact have a much smaller effect on the impulse redirection. A soft defect particle spatially localizes a small percentage of the incoming energy in the crystals, as it oscillates between its nearest neighbors. A stiffer defect particle redirects part of the incoming energy into single deflected and reflected solitary waves, and a simple rigid particle collision calculation was constructed for this case which describes the reflected, scattered and transmitted energy fractions in good agreement

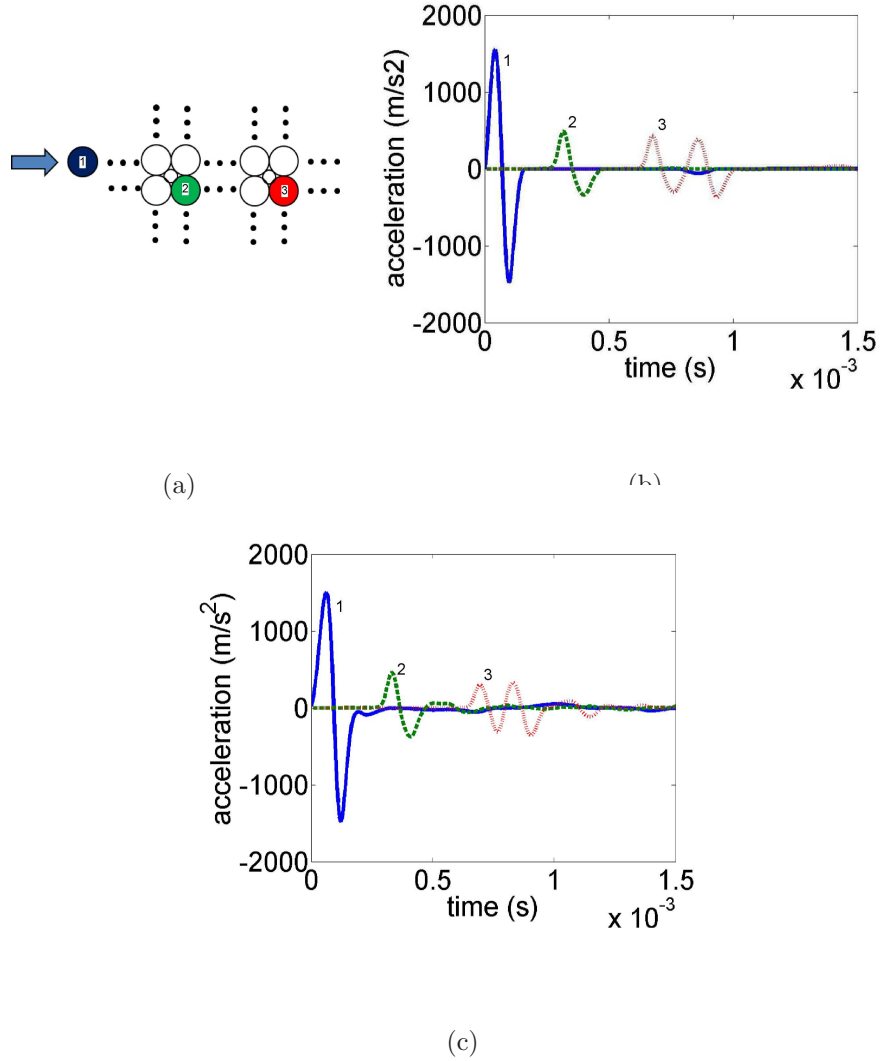


FIG. 11: (Color online) Comparison of the output accelerations observed experimentally (c) and numerically (b) for the configuration (a) when two tungsten carbide intruders are located 8 interstitial sites apart in a steel square packing impacted by a steel particle. After the incoming solitary wave (blue solid curve labeled “1”) interacts with the first defect, two waves travel towards the second defect: a transmitted wave in the impacted chain, and a redirected wave (green dashed curve labeled “2”) in the adjacent chain. The red dotted curve labeled “3” shows the two waves propagating after the second defect in the adjacent chain. The colors and labels of the particles correspond to the colors and labels of the acceleration curves in panels (c) and (b).

with numerical simulations and experimental results. The setting of two defects, placed in different configurations in the packing was also analyzed and it was noted that the energy

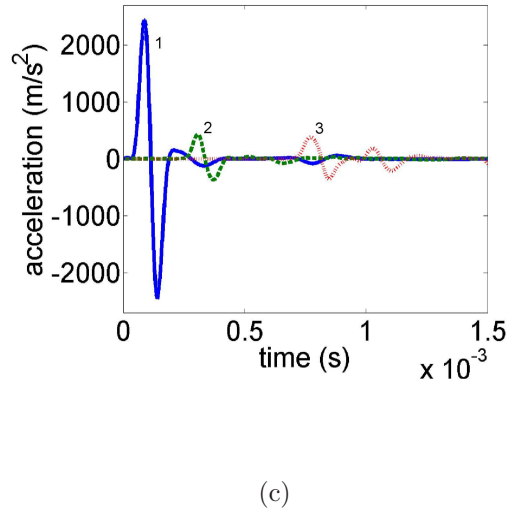
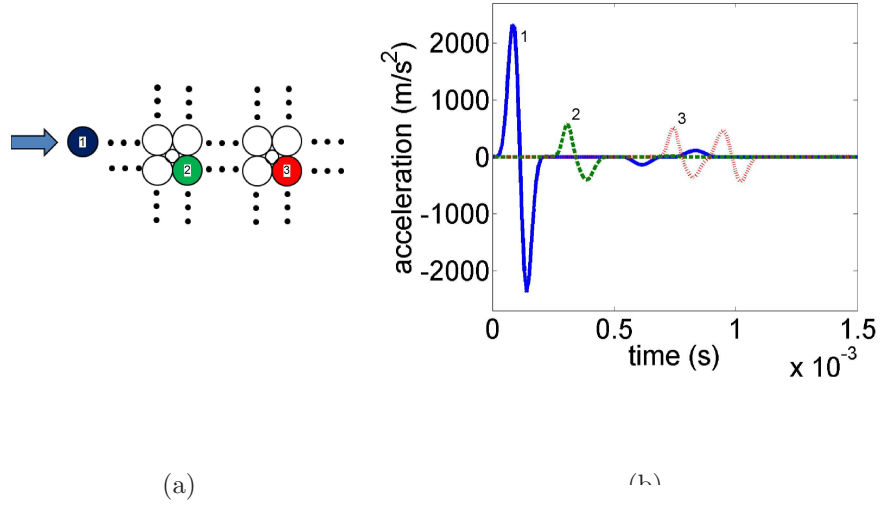


FIG. 12: (Color online) Comparison of the output accelerations observed experimentally (c) and numerically (b) for the configuration (a) when two tungsten carbide intruders are located 10 interstitial sites apart in a steel square packing impacted by a steel particle. After interaction of the incoming solitary wave (solid blue curve labeled “1”) with the first defect, two waves travel towards the second defect: a transmitted wave in the impacted chain, and a scattered wave (green dashed curve labeled “2”) in the adjacent chain. The red dotted curve labeled “3” shows the two waves propagating after the second intruder in the adjacent chain. The colors and labels of the particles correspond to the colors and labels of the acceleration curves in panels (c) and (b).

redirection efficiency of the system, measured as the amount of input energy not traveling along the impacted chain, is greatly enhanced when placing multiple defects in a line. If the defect particles are located far enough from each other (around 9-10 particles in our study), then they act independently and their individual behavior is identical to a single defect isolated in a square packing. This enabled a specific prediction for ensuring that the transmitted fraction stays below a prescribed fraction of the original energy. If the defect particles are located close to each other, their dynamic response is influenced by the respective presence.

The work presented in this paper provides a fundamental understanding of the effect of a single defect in 2-D granular crystals, and paves the way to more complex analyses involving a larger number of defect particles and especially a deeper understanding of their complex interplay. An ongoing project led by the authors consists of numerically investigating how the locations of these spherical intruders can be optimized to design new granular protecting devices, applying topology optimization techniques [44] to the type of systems considered herein.

## ACKNOWLEDGEMENTS

This work was supported by MURI grant US ARO W911NF-09-1-0436 (Dr. David Stepp is the grant monitor), and by the National Science Foundation (award number NSF/CMMI-844540-CAREER). We thank F. Fraternali, D. Tortorelli and M. Silva Sohn for useful discussions.

- 
- [1] V.F. Nesterenko, *J. Appl. Mech. Tech. Phys.* **24**, 733-743 (1983).
  - [2] A.N. Lazaridi and V. F. Nesterenko, *J. Appl. Mech. Tech. Phys.* **26**, 405-408 (1985).
  - [3] J.D. Goddard, *Proc. R. Soc. London, Ser. A*, **430**, 105-131 (1990).
  - [4] V.F. Nesterenko, *J. Phys. IV* **55**, C8-729 (1994).
  - [5] R.S. Sinkovits and S. Sen, *Phys. Rev. Lett.* **74**, 2686 (1995).
  - [6] S. Sen and R.S. Sinkovits, *Phys. Rev. E* **54**, 6857-6865 (1996).
  - [7] C. Coste, E. Falcon and S. Fauve, *Phys. Rev. E* **56**, 6104-6117 (1997).
  - [8] E.J. Hinch and S. Saint-Jean, *Proc. R. Soc. Lond. A* **455**, 3201-3220 (1999).

- [9] E. Hascoet, H.J. Herrmann and V. Loreto, *Phys. Rev. E* **59**, 3202-3206 (1999).
- [10] M. Manciu, S. Sen and A.J. Hurd, *Physica A* **274**, 588-606 (1999).
- [11] A. Chatterjee *Phys. Rev. E* **59**, 5912-5919 (1999).
- [12] R.S. MacKay, *Phys. Lett. A* **251**, 191-192 (1999).
- [13] M. Manciu, S. Sen and A.J. Hurd, *Phys. Rev. E* **63**, 016614 (2000).
- [14] V.F. Nesterenko, *Dynamics of Heterogeneous Materials* (Springer-Verlag, New-York, 2001).
- [15] C. Daraio, V.F. Nesterenko, E.B. Herbold and S. Jin, *Phys. Rev. E* **72**, 016603 (2005).
- [16] M. A. Porter, C. Daraio, E.B. Herbold, I. Szelenowicz and P.G. Kevrekidis, *Phys. Rev. E* **77**, 015601(R) (2008).
- [17] M. A Porter, C. Daraio, I. Szelenowicz, E.B. Herbold and P.G. Kevrekidis, *Physica D* **238**, 666-676 (2009).
- [18] S. Sen, J. Hong, J. Bang, E. Avalos and R. Doney, *Phys. Rep.* **462**, 21 (2008).
- [19] S. Sen, M. Manciu and J.D. Wright, *Phys. Rev. E* **57**, 2386-2397 (1998).
- [20] S. Sen, M. Manciu, R.S. Sinkovits and A.J. Hurd, *Gran. Matter* **3**, 33-39 (2001).
- [21] J. Hong, J.Y. Ji and H. Kim, *Phys. Rev. Lett.* **82**, 3058-3061 (1999).
- [22] M. Manciu, V.N. Tehan and S. Sen, *Chaos* **10**, 658-669 (2000).
- [23] C. Daraio, V.F. Nesterenko, E.B. Herbold and S. Jin, *Phys. Rev. E* **73**, 026610 (2006).
- [24] E.Hascoët and H.J. Hermann *Eur. Phys. J. B* **14**, 183-190 (2000).
- [25] S. Job, F. Santibanez, F. Tapia and F. Melo, *Phys. Rev. E* **80**, 025602(R) (2009).
- [26] M. Manciu, S. Sen and A.J. Hurd, *Physica A* **274**, 607-618 (1999).
- [27] V.F. Nesterenko, A.N. Lazaridi, and E.B. Sibiriyakov, *Journal of Applied Mechanics and Technical Physics* **36**, 166-168 (1995).
- [28] J. Hong and A. Xu, *Appl. Phys. Lett.* **81**, 4868 (2002).
- [29] J. Hong, *Phys. Rev. Lett.* **94**, 108001 (2005).
- [30] L. Vergara, *Phys. Rev. Lett.* **95**, 108002 (2005).
- [31] C. Daraio, V.F. Nesterenko, E.B. Herbold and S. Jin, *Phys. Rev. Lett.* **96**, 058002 (2006).
- [32] S. Job, F. Melo, A. Sokolow and S. Sen, *Phys. Rev. Lett.* **94**, 178002 (2005).
- [33] V.F. Nesterenko, C. Daraio, E.B. Herbold and S. Jin, *Phys. Rev. Lett.* **95**, 158702 (2005).
- [34] C. Hoogeboom, G. Theocharis and P.G. Kevrekidis, *Phys. Rev. E* **82**, 061303 (2010).
- [35] G. Theocharis, M. Kavousanakis, P.G. Kevrekidis, C. Daraio, M.A. Porter and I.G. Kevrekidis, *Phys. Rev. E* **80**, 066601 (2009).

- [36] D. T. Wu, *Physica A* **315**, 194-202 (2002).
- [37] M. Nakagawa, J.H. Agui, D.T. Wu and D.V. Extramiana, *Granular Matter* **4**, 167-174 (2003).
- [38] S. Sen, F.S. Manciu and M. Manciu, *Physica A* **299**, 551-558 (2001).
- [39] R. Doney and S. Sen, *Phys. Rev. E* **72**, 041304 (2005).
- [40] F. Melo, S. Job, F. Santibanez and F. Tapia, *Phys. Rev. E* **73**, 041305 (2006).
- [41] K. Lindenberg, U. Harbola, A.H. Romero and A. Rosas, *AIP Conf. Proc.* 1339 , 97-110 (2011).
- [42] L. Ponson, N. Boechler, Y.M. Lai, M.A. Porter, P.G. Kevrekidis and C. Daraio, *Phys. Rev. E* **82**, 021301 (2010).
- [43] F. Fraternali, M.A. Porter and C. Daraio, *Mechanics of Advanced Materials and Structures*, **17**, 1-19 (2010).
- [44] M.P. Bendsøe, O.Sigmund, *Topology Optimization*, Springer (2003).
- [45] H. P. Rossmanith, and A. Shukla, *Acta Mechanica* **42**, 211-225 (1982).
- [46] A. Shukla, M.H. Sadd, R. Singh, Q.M. Tai and S. Vishwanathan, *Optics and Lasers in Eng.* **19**, 99-119 (1993).
- [47] R. Singh, A. Shukla and H. Zervas, *Int. J. Solids Structures* **32**, 2523-2546 (1995).
- [48] B. Velický and C. Caroli, *Phys. Rev. E* **65**, 021307 (2002).
- [49] J.N. Roux, *Powders and Grains 97* (eds Behringer, R. P. and Jenkins, T. J.), 215-218 (1997)
- [50] S. G. Bardenhagen and J. U. Brackbill, *J. Appl. Phys.* **83**, 5732 (1998).
- [51] B. Gilles and C. Coste, *Phys. Rev. Lett.* **90**, 058002 (2006).
- [52] C. Coste and B. Gilles, *Phys. Rev. E* **77**, 021302 (2008).
- [53] A. Leonard, F. Fraternali and C. Daraio, *Experimental Mechanics*, Published Online (2011)  
DOI 10.1007/s11340-011-9544-6.
- [54] A. Leonard et al., *Proceedings of the Phononics 2011 International Conference on Phononic Crystals, Metamaterials and Optomechanics*, May 29-June 2, Santa Fe, NM
- [55] A. Leonard and C. Daraio, *Phys. Rev. Lett.* **108**, 214301 (2012).